Nanoscale Junction Formation by Gas-Phase Monolayer Doping

Peyman Taheri,[†,§] Hossain M. Fahad,[†,‡,§] Mahmut Tosun,[†,‡,§] Mark Hettick,[†,‡,§] Daisuke Kiriya,[†,‡,§] Kevin Chen,[†,‡,§] and Ali Javey*[,†,‡,§]

[†] Electrical Engineering and Computer Sciences, University of California, Berkeley, California 94720, United States [‡] Materials Sciences Division, Lawrence Berkeley National Laboratory, Berkeley, California 94720, United States [§] Berkeley Sensor and Actuator Center, University of California, Berkeley, California 94720, United States

Corresponding Author *E-mail: ajavey@berkeley.edu.

Abstract

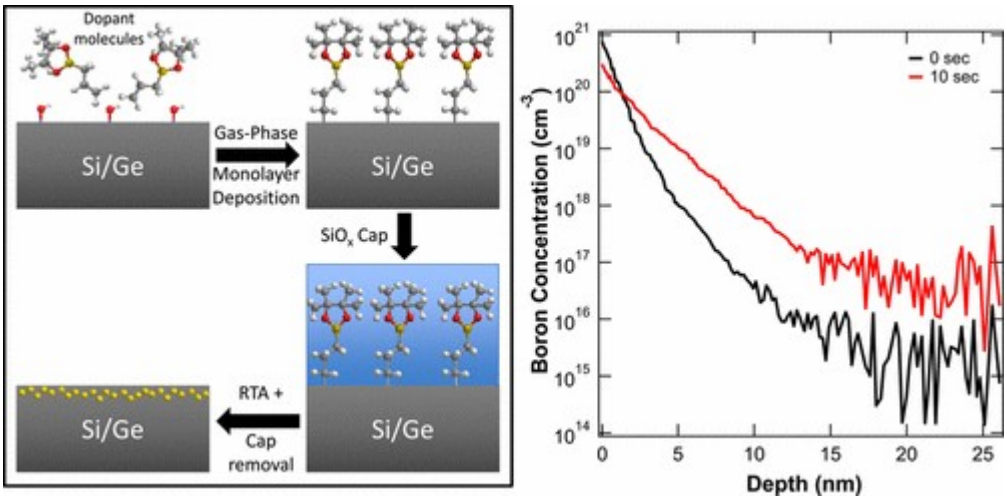

A major challenge in transistor technology scaling is the formation of controlled ultrashallow junctions with nanometer-scale thickness and high spatial uniformity. Monolayer doping (MLD) is an efficient method to form such nanoscale junctions, where the self-limiting nature of semiconductor surfaces is utilized to form adsorbed monolayers of dopant-containing molecules followed by rapid thermal annealing (RTA) to diffuse the dopants to a desired depth. Unlike ion implantation, the process does not induce crystal damage, thus making it highly attractive for nanoscale transistor processing. To date, reported MLD processes have relied on solution processing for monolayer formation. Gas-phase processing, however, benefits from higher intra- and interwafer uniformity and conformal coverage of 3D structures and is more desirable for manufacturing. In this regard, we report a new approach for MLD in silicon and germanium using gas-phase monolayer formation. We call this technology gas-phase monolayer doping (GP-MLD). This method relies on sequential pulse–purge cycles of gas-phase dopant-containing molecules to form a boron- or phosphorus-containing monolayer on a target semiconductor surface. Here, we show the feasibility of our approach through the formation of ultrashallow B- and P-doped junctions on Si and Ge surfaces. The mechanism of adsorption is characterized using Fourier transform infrared spectroscopy and X-ray

photoelectron spectroscopy. Sub-5 nm junction depths with high dopant dose are obtained as characterized by secondary ion mass spectrometry and sheet resistance measurements. Additionally, we demonstrate that area selectivity can be achieved via lithographic patterning of the monolayer dopants before the diffusion step. The results demonstrate the versatility of the GP-MLD approach for formation of controlled and ultrashallow junctions.

KEYWORDS: gas-phase monolayer doping, nanoscale junction, molecular adsorption, rapid thermal annealing, area-selective doping

Introduction

To meet the continuous demand for faster and more energy-efficient electronics, transistor scaling has been the main driving force for technology advancement in the semiconductor industry.(1-3) However, at the extreme scaling limit, a uniform surface doping profile in the transistor source and drain regions, channel, and subchannel becomes very important, especially for 3D semiconductor architectures such as fin field-effect transistors (FinFETs).(4, 5) The junction depth and dopant concentration should be well controlled to minimize contact resistance as well as variability effects due to random dopant fluctuations in the channel and subchannel regions of the FinFETs. As technology progresses to smaller nodes, conventional doping methods such as ion implantation suffer from deep junction creation, severe crystal damage, and incompatibility with 3D structures such as fins due to shadowing effects.(6, 7) Consequently, a well-defined, ultrashallow doping process is an urgent requirement with immediate technology benefits for today’s industry.

Previously, we developed a method known as monolayer doping (MLD) for controlled, nanoscale doping of semiconductor materials.(8-11) This method relies on (1) the formation of a monolayer of dopant-containing molecules on the semiconductor surface followed by deposition of a capping layer to encapsulate the molecules and (2) a subsequent thermal annealing step leading to bond cleavage and diffusion of dopant atoms to form a uniformly doped layer. This method takes advantage of the surface self-limiting chemisorption reactions to make covalent bonds between the dopant-containing molecules and Si surfaces which consequently allow control of the dopant profile on the surface by tuning the drive in conditions. Additionally, due to the monolayer formation process, MLD can be used for uniform doping of high aspect ratio nanostructures such as nanowires(12-14) and FINFETs.(15) Unlike ion implantation which can lead to damage and amorphization of the silicon surface due to bombardment of the surface with highly energized ions, MLD has been demonstrated for defect-free 20 nm FINFETs on the wafer scale.(16) In addition, the areal dopant dose for MLD can be well controlled by tuning the capping layer,(17) dopant molecule size, number of dopants per molecule,(18) as well as molecular surface coverage.(19) Due to the ability to form sharp, damage-free nanoscale junctions using this process, MLD has been proposed on the International Technology

Roadmap for Semiconductors (ITRS) as a potential doping process for future devices.(20)

One challenge in MLD is that the process requires appropriate solvents to form the monolayer surface termination. Industrialization of the process based on solution treatment is not favorable due to the lack of controllability and waste management issues. Here, we introduce a gas-phase monolayer doping (GP-MLD) method based on the formation of a monolayer of the dopant-containing molecules from the gas phase. The gas-phase deposition is desirable over solution processes for uniformity across multiple substrates and controllability of the monolayer formation process. In addition, gas-phase deposition removes the necessity for solvents and consequently the process wastes. Finally, gas-phase processing provides a more conformal and uniform coverage for 3D structures with high aspect ratio features. The GP-MLD process used for adsorption of dopant-containing molecules utilizes the equivalent of a half cycle in a conventional atomic layer deposition (ALD) process, without the counterpart pulse that oxidizes or reduces the surface layer. In order to saturate the substrate surface, multiple pulse–purge half cycles of the dopant molecule may be utilized. After deposition of the molecules on the semiconductor surface, a capping layer, e.g., SiO_x, is deposited to avoid loss of the adsorbed molecules during the subsequent drive-in step. The drive-in step utilizes a high-temperature spike anneal using either rapid thermal annealing (RTA) or a laser-based annealing process to drive the dopants into the desired depth. This is an efficient, self-contained, and reliable method to uniformly dope semiconductor surfaces over large areas, which is applicable for both p- and n-doping of nanostructured and planar surfaces for various applications.

Results and Discussion

Figure 1 schematically shows the GP-MLD process for Si and Ge substrates. Allylboronic acid pinacol ester and diethyl 1-propylphosphonate were used as the B- and P-containing precursors, respectively. Prior to introduction to the reactor chamber, silicon and germanium substrates were dipped into a 0.5% hydrofluoric acid (HF) solution for 5 s to remove the native oxide. The samples were then immediately transferred to a reactor chamber for the gas-phase molecular adsorption process. The samples were then capped with a 50 nm thick SiO_x layer deposited using electron-beam evaporation. RTA was then applied at various temperatures and times to drive the dopants into the desired depth. After drive in, the SiO_x capping layer was etched using a 0.5% HF solution, yielding an ultrashallow doped layer ready for immediate further processing.

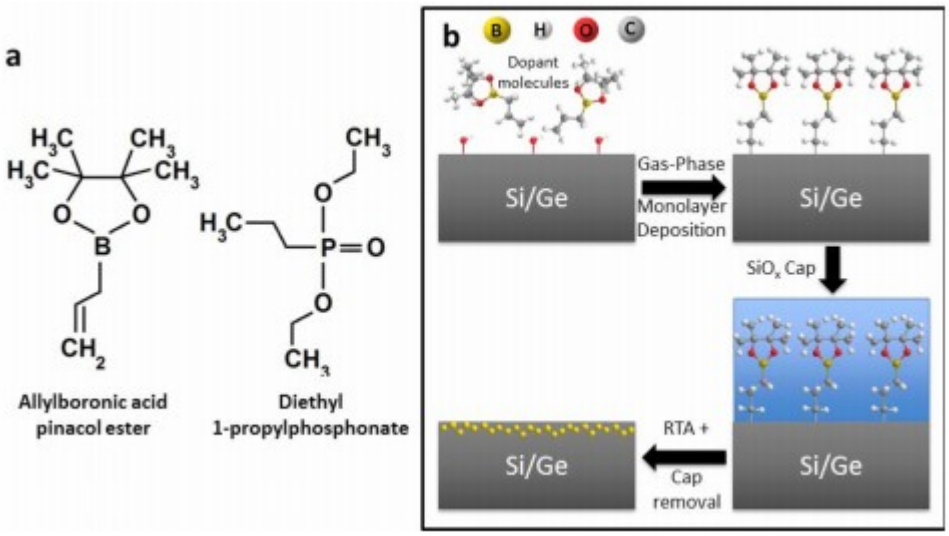

Figure 1. Schematic illustrations of the (a) allylboronic acid pinacol ester and diethyl 1-propylphosphonate precursors and (b) the gas-phase monolayer doping (GP-MLD) process of Si and Ge substrates using the allylboronic acid pinacol precursor.

Given the chosen molecules, we first explore the surface chemical structure and properties after the gas-phase monolayer formation process. Figure 2a shows the FTIR spectra of allylboronic acid pinacol ester on Si and Ge surfaces taken after monolayer deposition. The FTIR spectra show peaks around 2800–3000 cm^{-1}, corresponding to CH_2 and CH_3 stretching vibrations(21-23) originating from the interaction between allylboronic acid pinacol ester and the Si and Ge surfaces. On the other hand, the stretching vibration of C=C originating from intact molecules is expected to appear around 1650 cm^{-1}. The absence of such peaks indicates that the C=C bonds are opened upon interactions with the Si and Ge surfaces. The broad peaks around 1470 cm^{-1} can be assigned to different vibrational modes of the C–O bonds in the molecular structure. This indicates that the surface process involves a chemical interaction between the molecule and the surface resulting in alteration of the molecular structure and formation of stable surface–molecular bonds.

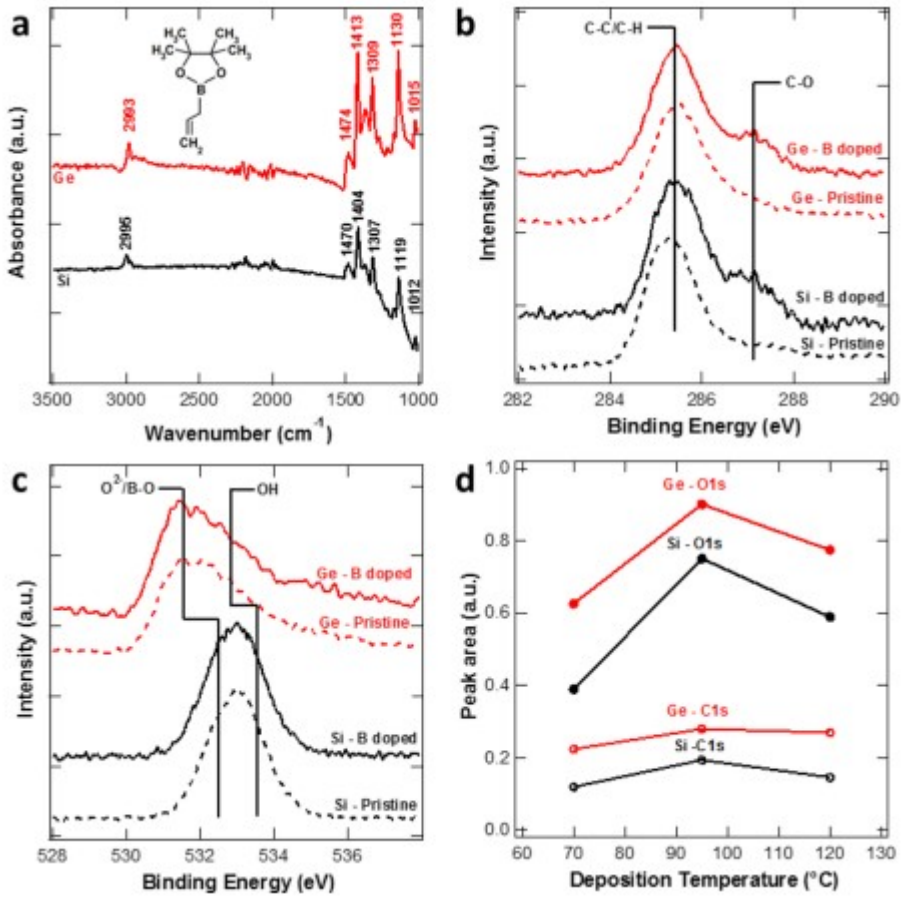

Figure 2. (a) FTIR spectra, (b) XPS C 1s, and (c) XPS O 1s spectra of allylboronic acid pinacol ester on Si and Ge substrates (deposition temperature was 95 °C). (d) Normalized C 1s, C–O and O 1s, O^{2-}/B–O subpeak areas of allylboronic acid pinacol ester on Si and Ge substrates at different deposition temperatures.

To further explore the interfacial interactions, XPS measurements were conducted on the surfaces before and after dopant deposition. For quantitative analyses, the XPS peaks are normalized versus reference Si 2P and Ge 2p peaks of the Si and Ge substrates, respectively, to subtract the measurement variations which may affect the signal intensities. Figures S1a and S1b show slight shifts of the Si $2P_{3/2}$ and Si $2P_{1/2}$ subpeaks and formation of shoulders for Ge $2P_{3/2}$ around 1221 eV and Ge $2P_{1/2}$ around 1252 eV subpeaks upon adsorption of the molecules as compared to the pristine samples (HF cleaned). These indicate that the surface chemistries of the Si and Ge surfaces are changed due to the GP-MLD process. Figures S1c and S1d, respectively, present the B 1s and P 2p spectra implying formation of the boron- and phosphorus-containing adsorbates. B 1s and P 2p peak intensities imply different amounts of adsorbates formed on Si and Ge substrates, while similar peak shapes indicate identical B and P bonding mechanisms on Si and Ge surfaces.

Figure 2b and 2c shows the XPS spectra for the C 1s and O 1s peaks, respectively. The C 1s peak is decomposed into C–C/C–H (285.4 eV) and C–

O^- (287.1 eV) species, while the O 1s peak is resolved into oxide and hydroxyl subpeaks indicating an ~1.5 eV difference in bonding energy.(24, 25) To calculate the actual hydroxyl fraction, the contribution of the surface contamination was subtracted according to the procedure described elsewhere.(26) The values of the C 1s and O 1s peak deconvolutions are summarized in Table 1. A plot showing the deconvoluted C 1s peaks for pristine and B-doped Si is shown in Figure S2 as an example. The C 1s spectra show a clear increase in the C–O subpeak area, indicating the presence of adsorbates on the surfaces. Additionally, the O 1s peaks show a reduction of the O–H peak area upon molecular adsorption, while the areas of the O^{2-}/B–O subpeaks increase. These indicate that the OH fraction of Si and Ge is consumed upon the molecular interaction, suggesting an acid–base interaction. These together with the FTIR results indicate that the chemisorption of allylboronic acid pinacol ester involves interactions between the carbon–carbon double bonds of the molecules and the −OH group of the surfaces, resulting in the formation of carbon–carbon single bonds. Consequently, the interaction of the allylboronic acid pinacol ester with the surfaces can be described by the following reaction

$$\mathrm{R{-}C{=}CH_2} + \mathrm{(Si/Ge){-}OH} \rightarrow \mathrm{R{-}C{-}C{-}(Si/Ge)} + \mathrm{H_2O} + 1/2\mathrm{H_2} \quad (1)$$

where R indicates the substitutional moieties on the molecule.

Table 1. Deconvoluted XPS C 1s and O 1s Peak Areas (%) for the Si and Ge Samples before and after Treatments with Allylboronic Acid Pinacol Ester Interaction

	C 1s		O 1s	
	C–C/C–H	C–O	O^{2-}/B–O	OH
Si pristine	92%	8%	45%	55%
Si–B doped	73%	27%	61%	39%
Ge pristine	90%	10%	39%	61%
Ge–B doped	82%	18%	52%	48%

Given knowledge of the surface chemical interaction, we explore the practical implications of the molecular surface arrangement and find an optimal parameter space for the deposition process. Figure 2d shows normalized subpeak areas of the C 1s, C–O and O 1s, O^{2-}/B–O subpeak areas of allylboronic acid pinacol ester on Si and Ge substrates versus the monolayer deposition process temperature. As discussed, these subpeaks are correlated to the molecular density on the Si and Ge surfaces. It can be seen that the greatest amount of adsorbates is obtained at a deposition temperature of 95 °C, whereas lower amounts of molecules are formed at 70 and 120 °C. An elevated temperature can increase the rate of desorption and reduce the number of defects in the formed monolayer while crossing the activation barrier for reorganization and lateral rearrangement of the adsorbates. However, further increasing the process temperature may cause phase changes and variations in the intermolecular interactions resulting in a

reduced amount of molecules adsorbed.(27-30) Therefore, it is found that a moderate temperature of 95 °C is optimal for this process.

Complementary to the boron-containing species, Figure 3 shows the FTIR and XPS spectra (C 1s and O 1s) of diethyl 1-propylphosphonate on Si and Ge surfaces. The FTIR spectra in Figure 3a exhibit peaks around 1000 cm^{-1} originating from P–O bonds, while those around 1400 cm^{-1} are correlated to C–H alkanes. Moreover, P═O phosphonate peaks within 1230–1260 cm^{-1} are small (or negligible), which indicates the formation of P–O bonds upon molecular adsorption on Si and Ge surfaces.(31-35) Similar to the boron case, the C 1s XPS peak shows a clear increase in the C–O peak intensity after monolayer deposition, indicating formation of adsorbates as shown in Figure 3b and Table 2. Like that of allylboronic acid pinacol ester, the O 1s XPS shows that adsorption of diethyl 1-propylphosphonate occurs along with hydroxyl removal, indicating an acid–base interaction. The OH reduction on Si upon molecular adsorption can be due to the interfacial interaction. On the other hand, the FTIR spectra indicate an interaction between the diethyl 1-propylphosphonate molecules and surfaces leading to formation of −P–O– bonds. The interaction of an unsaturated group, i.e., P═O, with the OH fraction suggests that the P═O group acts as the Lewis base (electron donor) and the OH as the Lewis acid (electron acceptor).(36) Simon et al.(37) and Majjane et al.(38) stated that the P═O bonding cleavage occurs during the interactions when the charge distribution of −P═O is displaced toward the oxygen atom, reducing the charge density around the P atom. Interaction of diethyl 1-propylphosphonate on Si and Ge surfaces can be shown as follows

$$\mathrm{R{-}P{=}O + (Si/Ge){-}OH \rightarrow R{-}P{-}O{-}(Si/Ge) + 1/2H_2O + 1/2O_2} \quad (2)$$

where R indicates the molecular moieties.

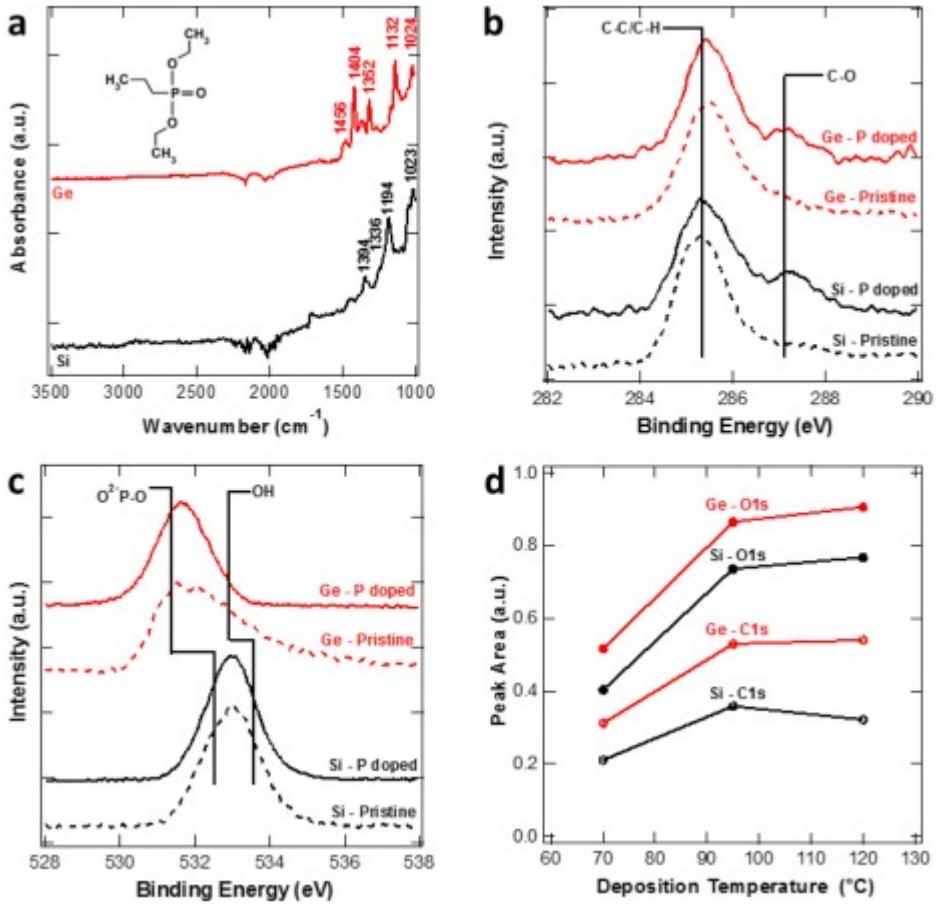

Figure 3. (a) FTIR spectra, (b) XPS, C 1s and (c) XPS, O 1s spectra of diethyl 1-propylphosphonate on Si and Ge substrates (deposition temperature was 95 °C). (d) Normalized C 1s, C–O and O 1s, O^{2-}/P–O subpeak intensities of diethyl 1-propylphosphonate on Si and Ge substrates at different temperatures.

Table 2. Deconvoluted XPS C 1s and O 1s Peak Areas (%) for the Si and Ge Samples before and after Treatments with Diethyl 1-Propylphosphonate Interaction

	C 1s		O 1s	
	C–C/C-H	C–O	O^{2-}/P–O	OH
Si pristine	92%	8%	45%	55%
Si–P doped	77%	23%	88%	12%
Ge pristine	90%	10%	39%	61%
Ge–P doped	86%	14%	94%	6%

Figure 3d exhibits the normalized C 1s, C–O and O 1s, O^{2-}/P–O subpeak areas of diethyl 1-propylphosphonate on Si and Ge substrates deposited at 70, 95, and 120 °C temperatures. Like that of allylboronic acid pinacol ester, the greatest amount of adsorbates is obtained at 95 °C, indicating the importance of a moderate temperature for optimal molecular adsorption using the GP-MLD process.

To demonstrate the effectiveness of the GP-MLD process for creating ultrashallow doped junctions, secondary-ion mass spectrometry (SIMS)

measurements were carried out on the Si samples doped with boron using the GP-MLD method. Figure 4 shows the B doping profiles of Si samples annealed at 1000 °C for 0 (i.e., spike anneal) and 10 s, indicating the formation of ultrashallow junctions. The surface boron concentrations in the samples are 7.5×10^{20} and 3×10^{20} cm^{-3} for the spike and 10 s anneals, respectively. For the spike anneal, the doping concentration decays abruptly at a rate of approximately 1.6 nm per decade, while for the 10 s drive in, the concentration decays slower at approximately 3.7 nm per decade due to the diffusion of dopants during the drive in. At a depth of 25 nm, the B concentration drops to 10^{15} and 10^{17} atoms/cm^3 for the spike anneal and 10 s drive in, respectively. In typical highly scaled transistors, the channel doping concentration is approximately 5×10^{18} cm^{-3}.(9) If the junction depth (x_j) is defined to be the depth at which the doping concentration is equal to 5×10^{18} cm^{-3} then this would correspond to an x_j of 3.5 and 11 nm, respectively, for the spike and 10 s drive in times. The nanoscale junctions demonstrated here are of particular interest for a wide range of applications such as highly scaled FinFETs and nanowire transistors given the known uniformity of gas-phase processes for conformal coverage of 3D structures.(39, 40)

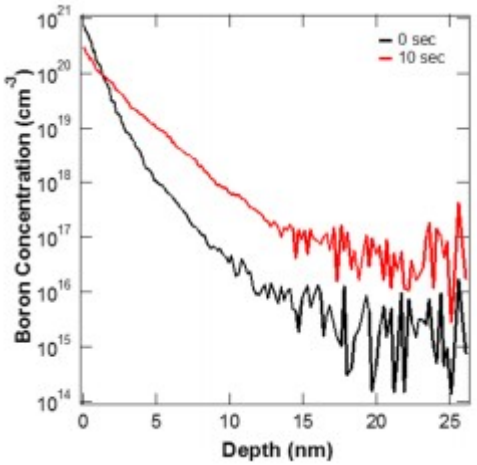

Figure 4. SIMS depth profiles of diffused boron atoms by GP-MLD in silicon wafers subjected to 0 s spike and 10 s RTA drive in at 1000 °C.

To further characterize the electrical performance of the doped samples, sheet resistance (R_s) measurements were conducted using the four-point probe technique for various RTA temperatures and times. The R_s values of the starting Si and Ge wafers used were 7×10^5 and 1500 Ω/□, respectively. Figure 5a and 5b shows the R_s values for the Si wafers doped with boron and phosphorus via GP-MLD as a function of annealing time for annealing temperatures of 950, 1000, and 1050 °C. It can be seen that for both dopants, the R_s values of the Si wafers sharply decrease with annealing time from 10^5–10^6 to 10^3–10^4 Ω/□ in all cases, with higher annealing temperatures leading to lower resistivities. This can be explained by more dopants being driven in over time followed by diffusion further into the Si surface. For longer annealing times, the resistivities increase slightly, which

presumably is due to deep diffusion and surface depletion of the dopants. Figure 5c and 5d shows the R_s values of boron- and phosphorus-doped Ge as a function of annealing time for annealing temperatures of 600, 650, and 700 °C. Lower drive-in temperatures were used for Ge as the diffusivity of B and P in Ge is much higher than that of Si. Similarly, the R_s values decrease with higher annealing temperatures due to the greater diffusivity. From these results it can be seen that by changing the diffusion temperature and time, the surface doping concentration as well as the junction depth can be tuned for different applications.

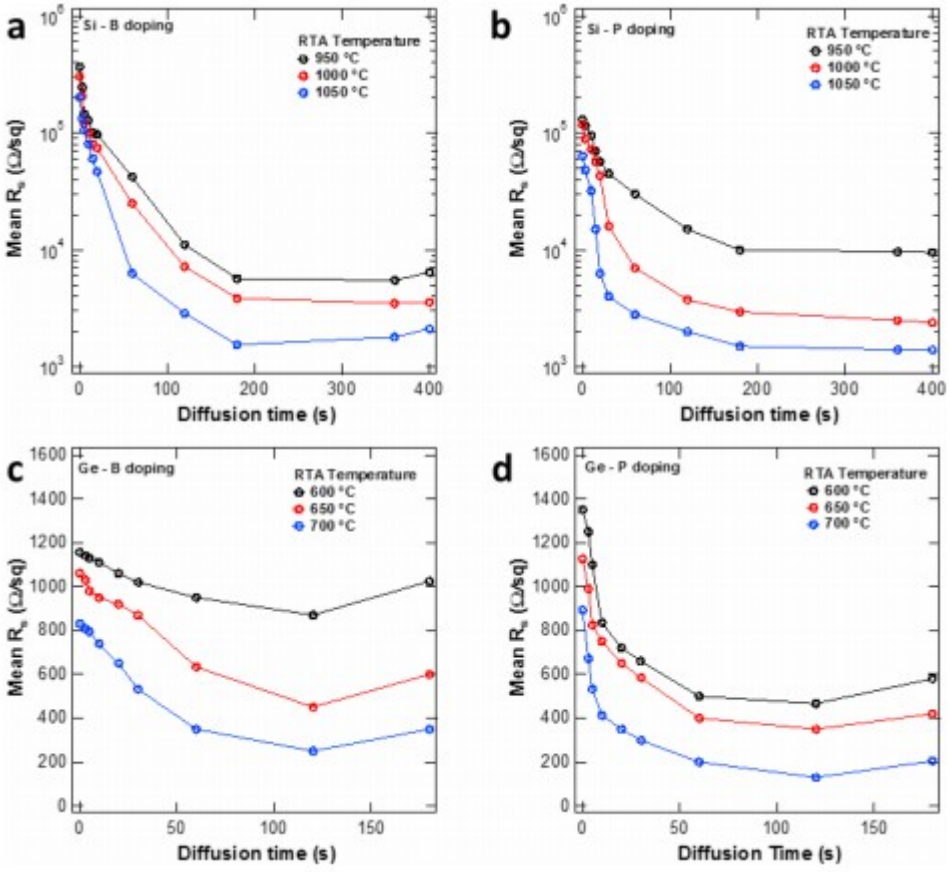

Figure 5. Sheet resistance of (a) B-doped Si wafer, (b) P-doped Si wafer, (c) B-doped Ge wafer, and (d) P-doped Ge wafer versus RTA annealing time at different temperatures, processed by GP-MLD.

For practical device applications, it is necessary to be able to achieve selective doping of certain areas rather than doping the entire surface of the device wafer. To demonstrate this, area-selective GP-MLD was conducted via patterning of a Si wafer. Figure 6a shows the fabrication process. The fabrication process consists of an electron-beam lithography step to pattern 2 µm squares with poly(methyl methacrylate) (PMMA) resist on the Si surface. Afterward, the molecular deposition of allylboronic acid pinacol ester was conducted after an immediate HF dip to remove native oxide using the gas-phase process followed by deposition of the SiO_x capping layer. Subsequently, the PMMA was lifted off in acetone, leaving dopant-free areas.

Then RTA was used to drive the dopants into the desired depth, and the SiO_x cap was removed. To characterize the effectiveness of the patterned doping, conductive AFM was used to map out the surface conductivity. Figure 6b shows a schematic of the conductive AFM setup, and Figure 6c shows example current–voltage curves taken on a doped and undoped region of the wafer, displaying an over 20× decrease in resistance in the doped region. Figure 6d shows the current and corresponding topography map from the AFM taken across the selectively doped regions at an ac bias voltage of 4.0 V. The conductive AFM image exhibits a sharp transition in conductivity between the doped and the undoped regions, demonstrating the feasibility of this process to be used in highly scaled devices. The topography image shows that the undoped regions are slightly raised compared to the doped regions, presumably due to the native oxide removal before the GP-MLD process.

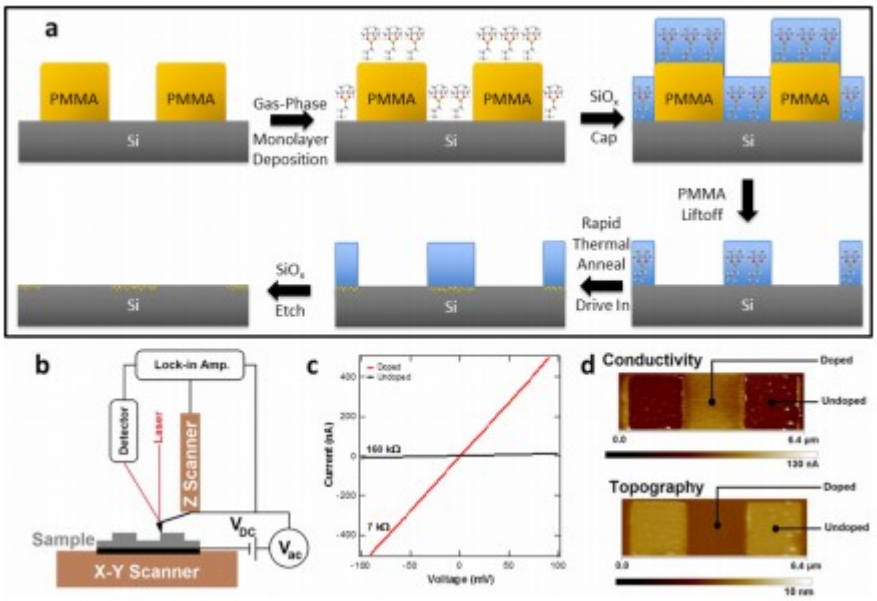

Figure 6. (a) Area-selective monolayer formation for patterned GP-MLD. (b) Schematic of a conductive AFM equipment. (c) Current–voltage curves taken from a doped and an undoped region on the patterned wafer. (d) AFM conductivity and topography maps of the doped and undoped regions.

Conclusion

In this work, we demonstrated monolayer doping of Si and Ge wafers by boron- and phosphorus-containing molecules via a gas-phase deposition process. The process, which we call gas-phase monolayer doping, utilizes a modified ALD apparatus to obtain fine control over surface saturation defined by a self-limiting surface reaction. We have shown that GP-MLD provides excellent controllability of the monolayer formation process and consequently well-defined areal dose and spatial distribution. Area-selective doping was conducted using lithography to pattern the deposited monolayers, the feasibility of which was verified using conductive AFM mapping. GP-MLD is of particular interest for a wide range of electronic applications enabling doping of ultrashallow junctions. In the future,

alternative B- and P-containing molecules with different active functional groups promoting selective adsorption on Si/Ge and their oxides may be explored. In this way, the areal dopant dose may be further controlled by utilizing molecules with different footprint size or by enabling controlled multilayer assembly by choosing the appropriate precursors.

Methods

Gas-Phase Monolayer Doping

The gas-phase monolayer doping tool is a home-built system resembling a conventional ALD apparatus consisting of a bottle containing precursor(s), a tube furnace reactor chamber, and gas delivery and pumping systems. The reactor temperature is set to 70, 95, and 120 °C for different samples. After reaching the set temperature, the precursor is pulsed 10 times for 1 s each with 20 s purge intervals to uniformly deposit a monolayer of the molecular dopant species onto the Si or Ge wafer. After deposition, the deposited monolayer is immediately capped with 50 nm of SiO_x, deposited via electron-beam evaporation to prevent desorption of the dopant molecules during the subsequent thermal diffusion step. Rapid thermal annealing (RTA) is conducted at temperatures between 950 and 1050 °C for doping of Si and between 600 and 700 °C for doping of Ge for either “0” (spike anneal) or 10 s. HF (0.5%) was used to remove the SiO_x cap after RTA drive in to complete the doping process. Since the quality of the capping layer, e.g., thickness, density, etc., can potentially influence the doping process, constant experimental parameters are used for deposition of SiO_x to obtain reproducible capping layers.

SIMS Measurements

The SIMS measurements were carried out using a Physical Electronics ADEPT-1010 quadrupole system. The depth scales were based on sputter rates calculated from the depths of the analytical craters, measured by stylus profilometry with NIST traceable calibration. Corrections to depth calibration, with changes in composition, have been applied (PCORSIMSSM) assuming a constant sputter rate for the entire profile. The one sigma accuracy of the depth calibration should be within ±1–10%. The concentration of B in Si was calibrated using sensitivity factors calculated from a standard sample. The B profiles were normalized on a point-to-point basis to the Si profile before the relative sensitivity factor was applied.(41)

Acknowledgments

P.T. was funded by the research programme 680-50-1301, which is financed by The Netherlands Organization for Scientific Research (NWO). XPS characterization was performed at the Joint Center for Artificial Photosynthesis, supported through the Office of Science of the U.S. Department of Energy under Award Number DE-SC0004993. Conductive AFM was measured by M. Savla using the PeakForce TUNA module on Dimension Icon AFM (Bruker Nano, Santa Barbara).

References

(1) Chau, R.; Doyle, B.; Doczy, M.; Datta, S.; Hareland, S.; Jin, B.; Kavalieros, J.; Metz, M. Silicon Nano-transistors and Breaking the 10 nm Physical Gate Length Barrier. Device Res. Conf. 2003, 123−126. (2) Lu, W.; Lieber, C. M. Semiconductor Nanowires. J. Phys. D: Appl. Phys. 2006, 39, R387−R406. (3) Wang, D.; Sheriff, B.; Heath, J. R. Silicon p-FETs from Ultrahigh Density Nanowire Arrays. Nano Lett. 2006, 6, 1096−1100. (4) Peercy, P. S. The Drive to Miniaturization. Nature 2000, 406, 1023−1026. (5) Claeys, C. Technological Challenges of Advanced CMOS Processing and their Impact on Design Aspects. VLSI Design 2004, 275−282. (6) Jones, E. C.; Ishida, E. Shallow Junction Doping Technologies for ULSI. Mater. Sci. Eng., R 1998, 24, 1−80. (7) Xiong, S.; Bokor, J. A Simulation Study of Gate Line Edge Roughness Effects on Doping Profiles of Short-channel MOSFET Devices. IEEE Trans. Electron Devices 2004, 51, 228−232. (8) Ho, J. C.; Yerushalmi, R.; Jacobson, Z. A.; Fan, Z.; Alley, R. L.; Javey, A. Controlled Nanoscale Doping of Semiconductors via Molecular Monolayers. Nat. Mater. 2008, 7 (1), 62−67. (9) Ho, J. C.; Yerushalmi, R.; Smith, G.; Majhi, P.; Bennett, J.; Halim, J.; Faifer, V.; Javey, A. Wafer-Scale, Sub-5 nm Junction Formation by Monolayer Doping and Conventional Spike Annealing.Nano Lett. 2009, 9 (2), 725−730. (10) Ho, J. C.; Ford, A. C.; Chueh, Y. L.; Leu, P. W.; Ergen, O.; Takei, K.; Smith, G.; Majhi, P.; Bennett, J.; Javey, A. Nanoscale Doping of InAs via Sulfur Monolayers. Appl. Phys. Lett. 2009, 95, 072108. (11) Cho, K.; Ruebusch, D. J.; Lee, M. H.; Moon, J. H.; Ford, A. C.; Kapadia, R.; Takei, K.; Ergen, O.; Javey, A. Molecular Monolayers for Conformal, Nanoscale Doping of InP Nanopillar Photovoltaics. Appl. Phys. Lett. 2011, 98, 203101. (12) Hazut, O.; Agarwala, A.; Subramani, T.; Waichman, S.; Yerushalmi, R. Monolayer Contact Doping of Silicon Surfaces and Nanowires Using Organophosphorus Compounds. J. Visualized Exp. 2013, 82, e50770. (13) Hazut, O.; Agarwala, A.; Amit, I.; Subramani, T.; Zaidiner, S.; Rosenwaks, Y.; Yerushalmi, R. Contact Doping of Silicon Wafers and Nanostructures with Phosphine Oxide Monolayers. ACS Nano 2012, 6 (11), 10311−10318. (14) Hazut, O.; Huang, B. C.; Pantzer, A.; Amit, I.; Rosenwaks, Y.; Kohn, A.; Chang, C. S.; Chiu, Y. P.; Yerushalmi, R. Parallel p−n Junctions Across Nanowires by One-step Ex Situ Doping. ACS Nano 2014, 8 (8), 8357−8362. (15) Lee, Y. J.; Cho, T. C.; Kao, K. H.; Sung, P. J.; Hsueh, F. K.; Huang, P. C.; Wu, C. T.; Hsu, S. H.; Huang, W. H.; Chen, H. C.; Li, Y.; Current, M. I.; Hengstebeck, B.; Marino, J.; Bü yü klimanli, T.; Shieh, J. M.; Chao, T. S.; Wu, W. F.; Yeh, W. K. A Novel Junctionless FinFET Structure with Sub-5nm Shell Doping Profile by Molecular Monolayer Doping and Microwave Annealing. 2014 IEEE International Electron Devices Meeting (IEDM), San Francisco, CA; IEEE, 2014. (16) Ang, K. W.; Barnett, J.; Loh, W. Y.; Huang, J.; Min, B. G.; Hung, P. Y.; Ok, I.; Yum, J. H.; Bersuker, G.; Rodgers, M.; Kaushik, V.; Gausepohl, S.; Hobbs, C.; Kirsch, P. D.; Jammy, R. 300mm FinFET Results Utilizing Conformal, Damage Free, Ultra Shallow Junctions (Xj ~ 5nm) Formed with Molecular Monolayer Doping Technique. 2011 IEEE International Electron Devices Meeting (IEDM), Washington, DC; IEEE, 2011. (17) Yum, J.

H.; Shin, H. S.; Hill, R.; Oh, J.; Lee, H. D.; Mushinski, R. M.; Hudnall, T. W.; Bielawski, C. W.; Banerjee, S. K.; Loh, W. Y.; Wang, W. E.; Kirsch, P. A Study of Capping Layers for Sulfur Monolayer Doping on III-V Junctions. Appl. Phys. Lett. 2012, 101, 253514. (18) Ye, L.; Gonzalez-Campo, A.; Nu´ ñ˜ ez, R.; de Jong, M. P.; Kudernac, T.; van der Wiel, W. G.; Huskens, J. Boosting the Boron Dopant Level in Monolayer Doping by Carboranes. ACS Appl. Mater. Interfaces 2015, 7 (49), 27357−27361. (19) Ye, L.; Pujari, S. P.; Zuilhof, H.; Kudernac, T.; de Jong, M. P.; van der Wiel, W. G.; Huskens, J. Controlling the Dopant Dose in Silicon by Mixed-Monolayer Doping. ACS Appl. Mater. Interfaces 2015, 7, 3231− 3236. (20) The International Technology Roadmap for Semiconductors (ITRS); http://www.itrs.net (accessed 2011). (21) Shustak, G.; Domb, A. J.; Mandler, D. Preparation and Characterization of n-alkanoic Acid Self-assembled Monolayers Adsorbed on 316L Stainless Steel. Langmuir 2004, 20, 7499−7506. (22) Tao, Y. Structural Comparison of Self-Assembled Monolayers of n-Alkanoic Acids on the Surfaces of Silver, Copper, and Aluminum. J. Am. Chem. Soc. 1993, 115, 4350−4358. (23) Nuzzo, R. G.; Dubois, L. H.; Allara, D. L. Fundamental Studies of Microscopic Wetting on Organic Surfaces. 1. Formation and Structural Characterization of a Self-consistent Series of Polyfunctional Organic monolayers. J. Am. Chem. Soc. 1990, 112, 558−569. (24) Briggs, D.; Seah, M. Practical Surface Analysis: Auger and X-ray Photoelectron Spectroscopy; Wiley: Chichester, 1990. (25) Taheri, P.; Hauffman, T.; Mol, J. M. C.; Flores, J. R.; Hannour, F.; de Wit, J. H. W.; Terryn, H. Molecular Interactions of Electroadsorbed Carboxylic Acid and Succinic Anhydride Monomers on Zinc Surfaces. J. Phys. Chem. C 2011, 115, 17054−17067. (26) Wielant, J.; Hauffman, T.; Blajiev, O.; Hausbrand, R.; Terryn, H. Influence of the Iron Oxide Acid−Base Properties on the Chemisorption of Model Epoxy Compounds Studied by XPS. J. Phys. Chem. C 2007, 111, 13177−13184. (27) Kawasaki, M.; Sato, T.; Tanaka, T.; Takao, K. Rapid SelfAssembly of Alkanethiol Monolayers on Sputter-Grown Au(111). Langmuir 2000, 16, 1719−1728. (28) Yamada, R.; Wano, H.; Uosaki, K. Effect of Temperature on Structure of the Self-assembled Monolayer of Decanethiol on Au(111) surface. Langmuir 2000, 16, 5523−5525. (29) Pivetta, M.; Pacchioni, G. E.; Fernandes, E.; Brune, H. Temperature-dependent Self-assembly of NC−Ph5−CN Molecules on Cu(111). J. Chem. Phys. 2015, 142, 101928. (30) Wang, Y.; Gao, X.; Xiao, Y.; Zhao, Q.; Yang, J.; Yan, Y.; Huang, J. Temperature Dependent Coordinating Self-assembly. Soft Matter 2015, 11, 2806−2811. (31) Fringeli, U. P.; Gunthard, H. H. Infrared Membrane Spectroscopy. Mol. Biol., Biochem. Biophys. 1981, 31, 270−332. (32) Garidel, P.; Blume, A.; Hubner, W. A Fourier Transform Infrared Spectroscopic Study of the Interaction of Alkaline Earth Cations with the Negatively Charged Phospholipid 1,2-Dimyristoyl-sn-glycero-3 Phosphoglycerol. Biochim. Biophys. Acta, Biomembr. 2000, 1466, 245− 259. (33) Yee, C.; Kataby, G.; Ulman, A.; Prozorov, T.; White, H.; King, A.; Rafailovich, M.; Sokolov, J.; Gedanken, A. Self-assembled Monolayers of Alkanesulfonic and Phosphonic Acids on Amorphous Iron Oxide Nanoparticles. Langmuir 1999, 15 (21), 7111−7115. (34) Gibson, I. R.; Best, S. M.; Bonfield, W. Chemical Characterization of

Silicon-substituted Hydroxyapatite. J. Biomed. Mater. Res. 1999, 44 (4), 422−428. (35) Shih, P. Y.; Yung, S. W.; Chin, T. S. FTIR and XPS Studies of P2O5-Na2O-CuO Glasses. J. Non-Cryst. Solids 1999, 244 (2−3), 211− 222. (36) Brogly, M.; Nardin, M.; Schultz, J. Evidence of Acid-Base Interfacial Adducts in Various Polymer/Metal Systems by IRAS: Improvement of Adhesion. J. Adhes. 1996, 58, 263−279. (37) Simon, V.; Muresan, D.; Takacs, A. F.; Neumann, M.; Simon, S.´ Local Order Changes Induced in Calcium−Sodium−Phosphate Glasses by Transition Metals. Solid State Ionics 2007, 178, 221−225. (38) Majjane, A.; Chahine, A.; Et-tabirou, M.; Echchahed, B.; Do, T.- O.; Mc Breen, P. X-ray Photoelectron Spectroscopy (XPS) and FTIR Studies of Vanadium Barium Phosphate Glasses. Mater. Chem. Phys. 2014, 143, 779−787. (39) Beckman, R. A.; Johnston-Halperin, E.; Melosh, N. A.; Luo, Y.; Green, J. E.; Heath, J. R. Fabrication of Conducting Si Nanowire Arrays. J. Appl. Phys. 2004, 96, 5921−5923. (40) Zhu, Z.-T.; Menard, E.; Hurley, K.; Nuzzo, R. G.; Rogers, J. A. Spin on Dopants for High-performance Single-crystal Silicon Transistors on Flexible Plastic Substrates. Appl. Phys. Lett. 2005, 86, 133507. (41) Kinoshita, A.; Tanaka, C.; Uchida, K.; Koga, J. High-performance 50-nm-gate-length Schottky-source/Drain MOSFETs with Dopantsegregation Junctions. VLSI Technology and Circuits, Kyoto, Japan, June 14−16, 2005; http://ieeexplore.ieee.org/stamp/stamp.jsp?arnumber= 1469250.